

Pre and post-cracking behavior of steel-concrete composite deck subjected to high cycle load

C. Fujiyama & K. Maekawa

The University of Tokyo, Tokyo, Japan

E. Gebreyouhannes

Addis Ababa University, Addis Ababa, Ethiopia

ABSTRACT: Structural performance of steel-concrete composite deck is simulated in using three dimensional nonlinear finite element analysis by incorporating the interface model that reproduces Mohr-Coulomb friction between steel and concrete. The composite mechanism with regard to the mechanical lock by steel ribs and interface friction is analyzed. First, the effect of interface friction is presented. Second, the process of internal crack of concrete is explained based on the mechanical interlock with different rib shapes. Finally, the effect of post-cracking behavior is examined by high-cycle fatigue analysis

1 INTRODUCTION

1.1 Background

Recent developments in the field of computer simulation technology have led to a renewed interest in fatigue problems of concrete. In Japan there has been a lot of reinforced concrete (RC) bridge decks damage reported since 1960. To work out from this problem, different groups of researchers installed a wheel-type moving load testing machine (Maeda & Matsui 1984). Various experiments have been conducted since 1980 (Matsui 1987, Pedikaris & Beim 1989). Based upon the results of these experimental studies, they could come up to several influencing factors in fatigue problems. Such as minimum thickness of slab and a certain requirement of rebar arrangement were renewed in design codes. It was effective in practical field.

Numerical analysis tackling this problem has been reported by Maekawa *et al.* (2006a). They have developed a three dimensional nonlinear finite element analysis framework "COM3" that fully traces mechanical damage and plasticity under high cycle repetition of loads in use of logarithmic accelerated time integration. The applicability of the analytical system has been verified for RC slabs under both high-cycle fixed and moving loads (Maekawa *et al.* 2006b).

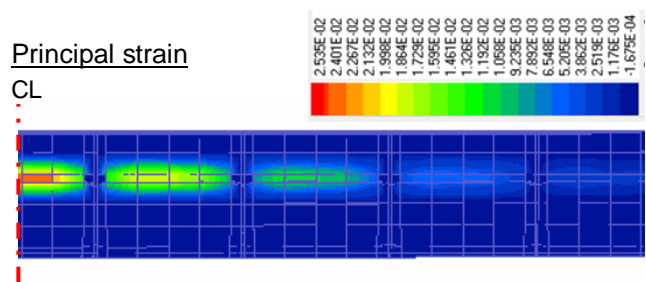
Engineers have been also developing interest to utilize steel-concrete composite slabs for bridge decks in the past decade. This is due to the fact that, this type of slab requires less amount of supporting girders in construction. Composite deck is of particularly application for use in a long span situation, where the use of RC slabs is not feasible.

As many bridge decks suffer from high-cycle moving loads, investigation of composite slabs subjected to high cyclic loads is required. Hawkins & Mitchell examined the response of composite slabs with different types of shear connectors under both monotonic and reversal cyclic shear (1984). They pointed out that failure mode is greatly influenced by the mechanical property of shear connector.

Sakurai *et al.* have examined the endurance limit of the composite deck that consists of bottom steel plates, steel ribs and concrete both experimentally and in using FE analyses (2005). Experimental results implied that a steel-concrete composite structure, which consists of the bottom steel plate, steel ribs and concrete, tends to start concrete crack from the tip of steel members under high-cycle loads.

Fujiyama & Maekawa analyzed the experiment done by Sakurai *et al.* using the enhanced model of "COM3" including the interface friction model for steel-concrete composite deck (2009). According to this study, progress of deflection has been successfully simulated as well as a particular crack development from the tip of steel ribs under the high-cycle moving loads as shown in Figure 1.

This paper focuses on the effect of composite mechanism on the cracking and post-cracking behavior of fatigue concrete. In particular, the effects of mechanical interlock by steel ribs, studs and the effect of interfacial friction is discussed extensively.



(a) Observed crack in experiment (Sakurai *et al.* 2005)

(b) Simulation by FE analysis (Fujiyama *et al.* 2009)

Figure 1. Internal crack of steel-concrete composite deck under high-cycle moving load.

	Compression	Tension	Shear transfer
Constitutive laws	<p>Stress - Strain</p> <p>$\sigma = E_0 K_0 \varepsilon_e$ $\varepsilon = \varepsilon_e + \varepsilon_p$</p>	<p>Stress - Strain</p> <p>$\sigma = E_c K_T \varepsilon_e$ $\varepsilon = \varepsilon_e + \varepsilon_p$</p>	<p>Shear stress - Slip or Strain</p> <p>$\tau = \int_{-\pi/2}^{\pi/2} R'_c(\omega, \delta, \theta) \sin \theta d\theta$</p>
Enhanced model for High cycle Fatigue	<p>Fracture parameter K_C considers time dependent plasticity & fracturing and cyclic fatigue damage</p> <p>$dK_C = \left(\frac{\partial K_C}{\partial t}\right) dt + \left(\frac{\partial K_C}{\partial \varepsilon_e}\right) d\varepsilon_e$</p> <p>Time dependency Cyclic fatigue</p> <p>$\left(\frac{\partial K_C}{\partial \varepsilon_e}\right) = \lambda \sim \text{when } F_k = 0$</p> <p>$\left(\frac{\partial K_C}{\partial \varepsilon_e}\right) = -\left(\frac{\partial F_k}{\partial \varepsilon_e}\right) \left(\frac{\partial F_k}{\partial K}\right) + \lambda \sim \text{when } F_k = 0$</p> <p>$\lambda = K^3 \cdot (1 - K^4) \cdot g \cdot R$</p> <p>EI-Kashif and Maekawa 2004</p>	<p>Fracture parameter K_T considers time dependent fracturing and cyclic fatigue damage</p> <p>$dK_T = F dt + G d\varepsilon_e + H d\varepsilon_e$</p> <p>Time dependent fracturing Cyclic fatigue damage</p> <p>Maekawa <i>et al.</i> 2003, Hisasue 2005</p>	<p>Accumulated path function X reduce shear associated with cyclic fatigue damage</p> <p>$\tau = X \cdot \tau_0(\delta, \omega)$</p> <p>function original model</p> <p>$X = 1 - \frac{1}{10} \log_{10} \left\{ 1 + \int \dot{d}(\delta/\omega) \right\} \geq 0.1$</p> <p>Contact density model by Li & Maekawa 1989, Modification of accumulated path function by Gebreyouhannes 2006</p>
Physical meaning	Decrease of stiffness and plasticity accumulation by continuous fracturing concrete	Decrease of tension stiffness by bond fatigue	Decrease of shear transfer normal to crack by continuous deterioration of rough crack surface

Figure 2. Internal crack of steel-concrete composite deck under high-cycle moving load.

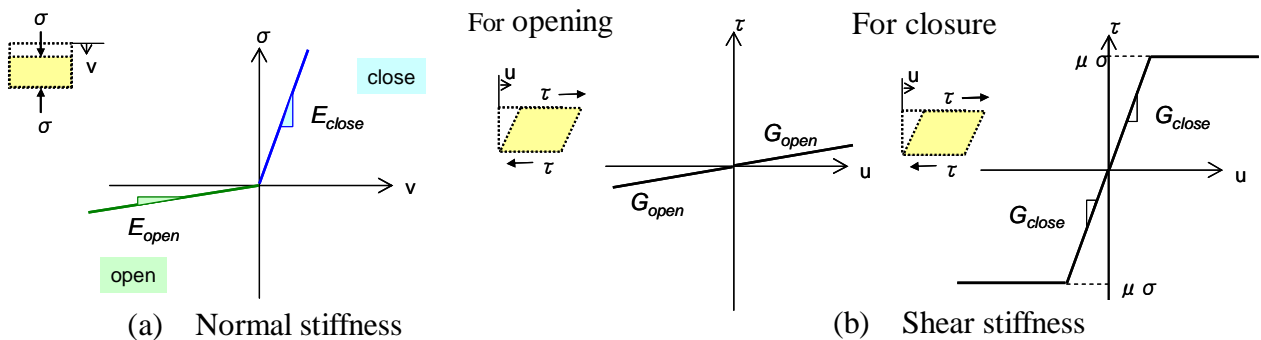


Figure 3. Interface friction model for steel-concrete composite structure.

1.2 Scheme of high cycle fatigue analysis

The fatigue simulation by "COM3" is based on the direct path integral scheme (Maekawa *et al.* 2003). Three basic essential models for concrete used herein are compression, tension and crack shear models along crack planes. These three models are of importance to treat the cumulative fatigue damages and time dependent effects (Fig. 2.). Simulation is conducted by tracing the evolution of microscopic material states at each moment. Logarithmic integral method accelerates computing for high cycle problem as well.

For full 3D simulation, Maekawa *et al.* has extended in-plane 2D RC models including time dependency and creep to 3D orthogonal space system by means of the projection-composition method (2003). This composition technique is regarded as a simple extension of the multi-directional non-orthogonal fixed crack approach. This computational framework has already been verified under low-cycle static and dynamic loads. Whatever the complexity of the loading hysteresis is, the multi-axial stress-carrying mechanism is formulated as a linear combination of 1D sub-mechanisms representing the cracked concrete and reinforcement as proposed by Collins & Vecchio (1982).

To replicate the actual stress transfer between the steel members and concrete, interface element is proposed with mechanical properties as indicated in Figure 3. The behavior is based upon Coulomb's friction law. The friction coefficient is assumed to be constant during loads. The interface model does not take into account the reduction of stiffness and residual strain due to high cycle loading.

2 MECHANISM OF COMPOSITE ACTION

2.1 Composite deck model

The steel-concrete composite deck investigated here consists of bottom steel plate, I-shape steel ribs, reinforcing bars and concrete. The model is simply supported on two sides in the vertical direction. The in-plane dimension of the slab is 1.5 m x 1.5 m having a gross depth of 169 mm, including 9 mm thick bottom plate.

I-shape steel ribs are set only in the transverse direction of 300 mm spacing. Ribs have neither studs nor holes for interlocking with surrounding concrete. Ribs are welded to the bottom plate and any other shear connector does not exist in this deck. Interface element model is proposed for the contact surface between steel plates and concrete as indicated in Figure 3. According to Rabbat and Russell (1985), the frictional coefficient for normal strength concrete with dry condition, can be assumed to be 0.6, as a constant. The current interface model does not take

into account the reduction of stiffness and residual strain due to high cycle loading.

Reinforcing bars consisting of D13c/c250 mm in the longitudinal direction provide single RC layers on the I-shape rib, and cover depth of reinforcing bars is 42 mm. Reinforcing bars and concrete above the ribs are modeled as RC element with bond effect. The other concrete parts are regarded as plain concrete. Tension stiffening/softening factor is determined for each concrete element. Figure 4 shows steel frame of this slab and the cross section of ribs. Table 1 shows mechanical properties of respective materials.

2.2 Composite mechanism

Steel-concrete composite mechanism consists of two actions in general. One is the mechanical interlock owing to shear connectors, such as ribs and studs. Another one is the interfacial friction between steel and concrete. Both mechanical stress-transfer and the interfacial friction contribute to consistent kinematics of steel and of concrete.

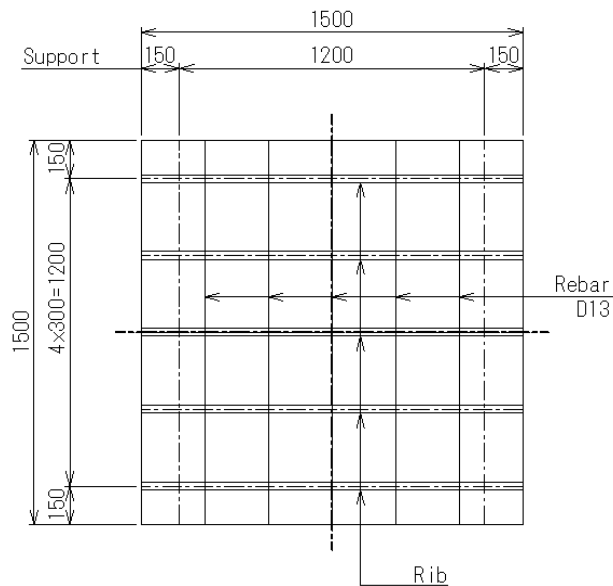
The composite deck investigated here can be an appropriate example to analyze these mechanisms. Interlocking by steel ribs acts as the main stress transfer mechanism across ribs. The effect of interface friction of the bottom plate should be included to this stress transfer mechanism as well, no matter how minor role it has in this direction. In contrast, the interfacial friction is the sole stress transfer mechanism along the ribs because of no shear connectors in this direction.

To examine the abovementioned stress transfer mechanisms on the structural performances, the authors set four models for analysis (see Table 2). Type-I series has I-shaped ribs (section 2.1). Type-F series has rectangular ribs (Fig. 4.). The height of the rib is 105mm which is the same as that of the prototype. The thickness of rib is made to be 18mm so as to have equivalent moment of inertia with that of the I-shaped rib. Flat plate rib changes stress concentration and crack initiation inside concrete, even though its stiffness is equivalent to that of the I-shaped rib. Extreme small friction coefficient, 0.1, also changes stress concentration and crack initiation inside concrete. The number -06 and -01 stand for the friction coefficient, 0.6 and 0.1 respectively.

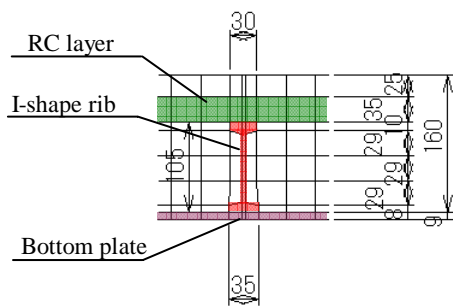
3 ANALYSIS FOR INTERNAL CRACKING

3.1 The effect of interface friction

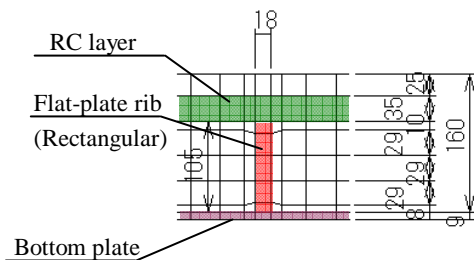
The static load is applied by displacement control at a rate of 0.2 mm/sec. The load is applied on a 200mm square area at the center of the slab. A maximum displacement of 40 mm is applied before the complete unloading.



(a) Dimension of analysis model



(b) I-shape rib (I-06, I-01)



(c) Flat-plate rib (F-06, F-01)

Figure 4. Steel-concrete composite deck model for FE analysis.

Table 1. Material properties of analysis model.

Name	Strength N/mm ²	Stiffness N/mm ²	ν	
Concrete	Compression	36.0	3.0×10^4	
	Tension	2.5		
Rebar (D13)	Yield point	400.0	2.0×10^5	0.30
Bottom plate	Yield point	350.0	2.0×10^5	0.30
I-shape rib	Yield point	400.0	2.0×10^5	0.30

Table 2. Cases for FE analysis.

Case	I-shape rib	Flat-plate rib
Fiction coefficient $\mu=0.6$	I-06	F-06
	Prototype	
$\mu=0.1$	I-01	F-01

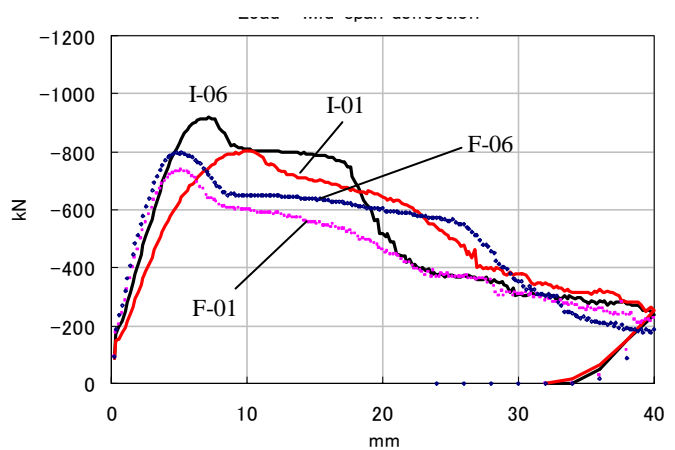


Figure 5. Load - Mid-span deflection.

Table 3. Summary of static analysis.

Name	Capacity kN	Deflection mm	Bottom plate Principal strain μ
I-06	917	7.2	1353
I-01	804	10.0	1964 (yield)
F-06	798	5.2	1113
F-01	736	5.2	1301

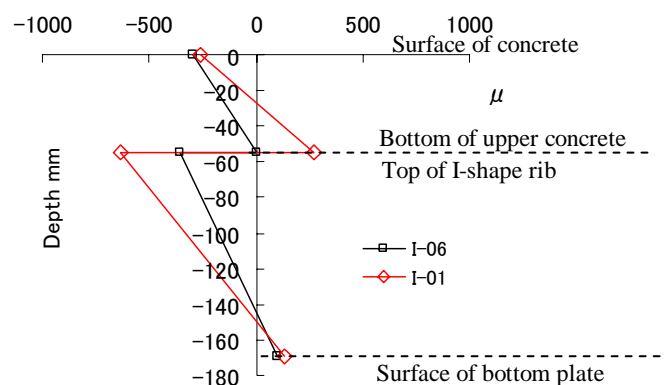
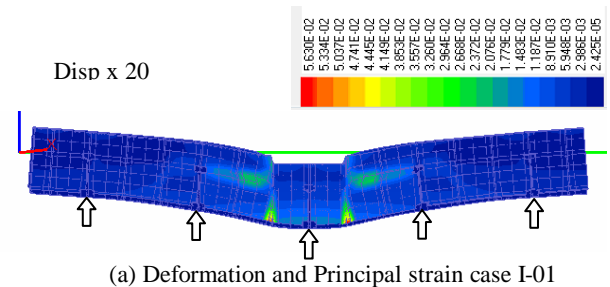
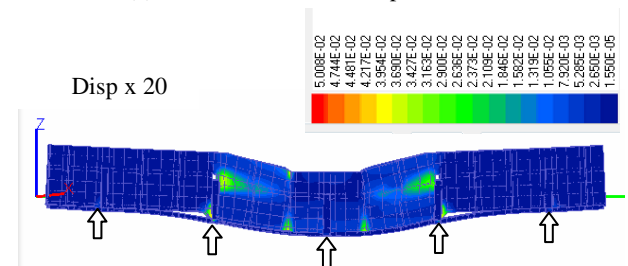


Figure 6. Strain distribution along rib at the center of span.



(a) Deformation and Principal strain case I-01



(b) Deformation and Principal strain case F-01

Figure 7. Strain distribution along rib at the center of span.

Figure 5 shows the load versus mid-span deflection curve under the static loading for all cases. For each case, the static capacity, mid-span deflection and the maximum principal strain of the bottom plate at the peak load are summarized in Table 3. Case I-06 shows 113 kN higher capacity and somewhat stiffer response than that of case I-01.

The stiffness of case I-01 starts to decrease around 200 kN. This reduction indicates slipping at the interface between concrete and the steel plate, as a result of low friction coefficient, 0.1. Figure 6 shows the strain along the rib at mid-span cross section at a load of 200 kN. Case I-01 shows a noticeable slip, showing a difference in strain of 909μ between top of steel and upper concrete. Even though the strain of surface concrete and that of the bottom plate are almost the same as that of case I-06.

Moreover, the different property of interfacial friction has a correlation with failure mode. As indicated in Table 3, the principal strain at the peak load of case I-01 exceeds yielding point, although that of case I-06 does not reach yielding. This means that the low friction case I-01 fails not only by punching shear of concrete but also by yielding of the bottom steel plate.

3.2 The effect of mechanical lock by steel ribs and internal crack

Case F-06 shows 62 kN higher capacity than that of F-01. The difference is due to the difference of interface friction, even though the stiffness does not show clear difference. Figure 7 shows 20 times magnified deformation and the principal strain distribution at the peak load. To focus on the effect of the mechanical interlock of steel ribs, case I-01 and case F-01, which has 0.1 of the interfacial friction coefficient are compared.

Figure 7(a) illustrates localization of tensile strain as vertical cracks under the loading area and as horizontal cracks in a layer including flange of ribs. The reason why the horizontal crack develops is that compressed upper concrete just under the loading area causes severe shear deformations to surrounding concrete in the layer including flange of ribs.

Figure 7(b) shows localization of tensile strain around the tip of ribs. This local deformation creates the horizontal internal crack from the tip of ribs. In addition, we can see openings between concrete and the bottom plate as well as between concrete and the top of ribs. The rectangular rib without flange does not restrain concrete in the vertical direction. This indicates that I-shape ribs with flange provide more efficient mechanical interlock, owing to their shape as compared to the rectangular ribs.

On the basis of this analysis, the combination of interface friction and the mechanical lock is considered. F-01 and F-06 cause the openings between

concrete and steel in the early stage because of insufficient confinement in the vertical direction. The interface friction along the rib seems to have a minor role for this opening. The stiffness mainly depends on the mechanical property of the steel parts after this opening. That is the reason why the difference in stiffness is not observed clearly between F-01 and F-06 as shown in Figure 5.

4 POST-CRACKING SUBJECTED TO HIGH-CYCLE MOVING LOAD

4.1 Condition for analysis

High-cycle moving load is applied on a 500 mm width and 1000 mm length of the mid-span to the cases I-06 and F-06. The load level is about 55 % of static capacity of the prototype, I-06. The moving speed is set as 4.0 m/s.

In addition, another case study of TS-06 is proposed. The tension stiffening/softening factor c of plane concrete element is changed from 1.5 to 0.4 in the vertical direction for TS-06. Dimension and property of steel parts are totally the same as that of I-06. However, this improvement does not contribute to increasing bond between steel and concrete, this improvement increases restraint of post-cracking concrete in the vertical direction without altering the interlocking mechanism. Increasing confinement in the vertical direction improves shear transfer across the horizontal crack under high-cycle loads. The tension stiffening/softening factor c is explained as follows;

$$\sigma_t = f_t \left(\frac{\varepsilon_{tu}}{\varepsilon_t} \right)^c \quad (1)$$

where σ_t = average concrete stress in tension; f_t = uniaxial tensile strength of concrete; ε_{tu} = average concrete strain at which crack occurs; ε_t = average concrete strain; and c = tension stiffening/softening factor (Maekawa *et al.* 2003). Generally speaking, $c = 0.4$ is used for concrete with deformed bar.

The authors think that tension stiffening/softening factor can be improved not only with deformed bar or but also with some amount of fiber material in practice. Abrishami and Mitchell (1997) experimentally demonstrated the improvement of post-cracking behavior of reinforced concrete in uniaxial tension by using 1% fiber by volume of concrete.

4.2 Fatigue life of deck and failure mode

Figure 8 shows progress of the computed mid-span deflection versus number of moving load cycles. The maximum deflection during the first cycle is 2.7 mm for TS-06 and is 2.8mm for I-06. This difference increases from 0.1 mm to 3.1 mm (TS-06; 5.5mm, I-

06; 8.6mm) after 100,000 cycles. This means that the post-cracking of concrete strongly affects the long-term structural performance, even if it does not give significant influence on the structural performance of the very beginning.

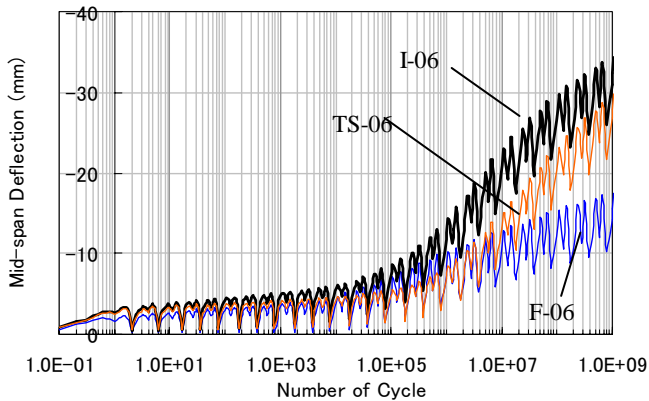
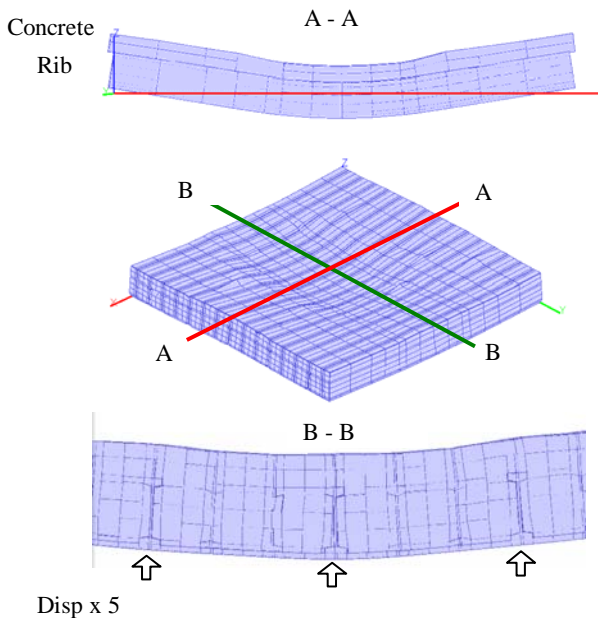
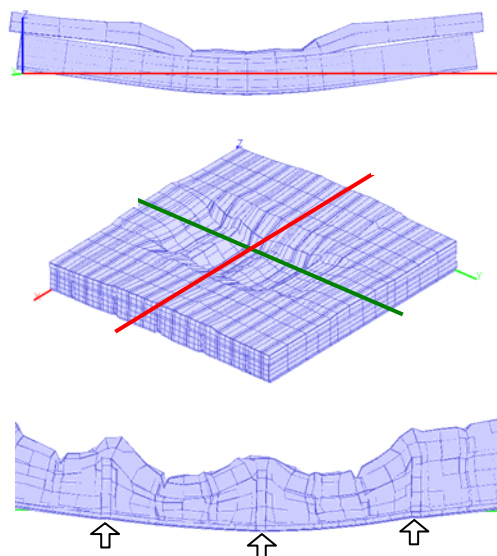


Figure 8. Progress of mid-span deflection under moving load.



(a) Deformation at 10,000,000 cycles, case TS-06



(b) Deformation at 10,000,000 cycles, case F-06

Figure 9. Deformation at 10,000,000 cycles of moving load.

Observable deformation of concrete as well as the gap opening between concrete and rib can be clearly seen in Figure 9(b). The maximum principal strain of the bottom plate is 2289μ . This means that concrete and the flat-plate rib do not act together without locking system in the vertical direction. This induces failure of both steel and concrete. The structural consistency is damaged.

The maximum principal strain of bottom plate is 2289μ . This means that concrete and flat-plate rib do not act together without locking system in vertical direction. This induces failure of both steel and concrete.

According to this study, performance of the composite decks should be evaluated not only by the mid-span deflection but also by damage of concrete due to high-cycle fatigue loads. Fatigue failure of the upper concrete fiber really affects the service life of composite bridge decks.

5 CONCLUSIONS

Structural performance of steel-concrete composite deck is simulated in using a three dimensional non-linear finite element analysis that fully traces mechanical damage and plasticity of concrete under high cycle repetition of loads in use of logarithmic accelerated time integration. Interface model is used to reproduce the Mohr-Coulomb's friction between steel and concrete.

The authors investigated the composite mechanism with regard to the mechanical interlock and the interfacial friction and examined their contribution to the whole performance by using the static analysis. First, the effect of interface friction is addressed. Second, the process of internal crack of concrete is explained based on the mechanical interlock by considering different rib shapes. Finally, the effect of post-cracking behavior is examined in using high-cycle fatigue analysis. The main conclusions are listed as;

Composite decks with assumed interface frictional coefficient $\mu = 0.1$ shows more than 10 % lower static capacity than that of the prototype ($\mu = 0.6$) for the cases of I-shape steel ribs.

The composite deck, which has the assumed interface frictional coefficient $\mu = 0.1$, shows more than 30% lower stiffness than that of the prototype ($\mu = 0.6$) for the case of I-shape steel rib.

The rectangular rib, which is designed to have equivalent moment of inertia as that of the I-shaped rib, shows about 10 % lower static capacity than that of the prototype (I-shaped rib).

The rectangular rib causes stress localization around its tip, and this localization causes internal cracking of concrete.

In the absence of vertical restraint due to mechanical interlocking, the vertical opening at the interface between steel and concrete is observed computationally.

Increasing confinement of concrete in the vertical direction improves the long-term structural performance under high-cycle moving loads.

As the flat-plate rib does not provide the mechanical locks in the vertical direction, concrete and steel ribs do not move together as a consistent manner. The high-cycle moving load causes serious damage not only to concrete between steel ribs but also to the steel itself.

6 ACKNOWLEDGEMENT

The authors express their gratitude to Dr. Benny Suryanto of The University of Tokyo for his valuable discussion. The authors' deep appreciation is extended to the financial supports from Global COE project on Urban Regeneration in The University of Tokyo. This work was supported by JSPS Grant-in-Aid for scientific research (A) No. 80157122 and JSPS Grant in Aid for research fellowship for young scientists No.20-56191.

REFERENCES

- Abrishami, H. H. & Mitchell, D. 1997. Influence of Steel Fibers on Tension Stiffening. *ACI Structural Journal* 94(6): 769-776.
- Collins, M. P. & Vecchio, F. 1982. The response of reinforced concrete to in-plane shear and normal stresses. University of Toronto.
- Hawkins, M. N. & Mitchell, D. 1984. Seismic response of composite shear connectors. *Journal of Structural Engineering* 110(9): 2120-2136.
- Fujiyama, C. & Maekawa, K. 2009. A numerical analysis of damage mechanism of bridge deck slab under high cycle moving load. *Proceedings of Second International Conference on Fatigue and Fracture in the Infrastructure 2009*.
- Maeda, Y. and Matsui, S. 1984. Fatigue of reinforced concrete slabs under trucking wheel load. *Proceedings of JCI* 6: 221-224.
- Matsui, S. 1987. Fatigue strength of RC-slabs of highway bridge by wheel running machine and influence of water on fatigue. *Proceedings of JCI* 9(2): 627-632.
- Maekawa, K., Toongoenthong, K., Gebreyouhannes, E. and Kishi, T. 2006a. Direct path-integral scheme for fatigue simulation of reinforced concrete in shear. *Journal of Advanced Concrete Technology* 4(1): 159-177.
- Maekawa, K., Gebreyouhannes, E., Mishima, T. and An, X. 2006b. Three-dimensional fatigue simulation of RC slabs under traveling wheel-type loads. *Journal of Advanced Concrete Technology* 4(3): 445-457.
- Maekawa, K., Fukuura, N. and Soltani, M. 2008. Path-Dependent High Cycle Fatigue Modeling of Joint Interfaces in Structural Concrete. *Journal of Advanced Concrete Technology* 6(1): 227-242.
- Pedikaris, P. C. & Beim, S. R. 1989. RC bridge decks under pulsating and moving load. *Journal of Structural Engineering* 114(3): 591-607.
- Rabbat, B. G. & Russell, H. G. 1985. Friction Coefficient of Steel on Concrete or Grount. *Journal of Structural Engineering* 111(3): 505-515.
- Sakurai, N., Fujikawa, K., Mizukami, S., Matsui, S. and Nagai, M. 2005. A study on rationalization of the shape steel bridge. *Journal of JSCE* 794: 67-86.